Coexistence of *G*- and *C*-type orbital ordered phases and its correlation with magnetization reversal in YVO_3

Rana Saha,[1] Francois Fauth,[2] Vincent Caignaert,[3] and A. Sundaresan[1,*]

[1]*Chemistry and Physics of Materials Unit and International Centre for Materials Science, Jawaharlal Nehru Centre for Advanced Scientific Research, Jakkur P.O., Bangalore 560 064, India*

[2]*CELLS-ALBA Synchrotron, E-08290 Cerdanyola del Vallès, Barcelona, Spain*

[3]*CRISMAT, UMR 6508, CNRS-ENSICAEN, 6 Bd Marechal Juin, 14050 Caen, France*

(Received 10 December 2016; revised manuscript received 5 April 2017; published 19 May 2017)

It is known that the orbital disordered orthorhombic ($Pnma$) perovskite, YVO_3, undergoes a transition to the G-type orbital ordered monoclinic phase ($P112_1/a$) at $T_{G\text{-OO}} \sim 200$ K followed by a first-order transition to the C-type orbital ordered orthorhombic phase ($Pnma$) at $T_S \sim 77$ K. In contrast, using the high-angular-resolution synchrotron x-ray powder diffraction technique, we find that the C-type orbital ordered phase appears at $T_N = 116$ K and coexists with the G-type monoclinic phase down to $T_S \sim 77$ K. The coexistence of different orbital ordered states in the temperature range $T_S < T < T_N$ is discussed based on large octahedral distortion caused by smaller Y ions present at the A site of the perovskite. Intriguingly, the temperature evolution of the coexistence of the G- and C-type orbital ordered phases and associated magnetic structures could be responsible for the temperature-induced magnetization reversal observed in the temperature interval $T_S < T < T_N$. We also discuss that the correlation of phase coexistence and magnetization reversal is present in other RVO_3 systems.

DOI: 10.1103/PhysRevB.95.184107

I. INTRODUCTION

The orthovanadate RVO_3 (R = rare earth and Y) family of compounds with the perovskite structure provides an interesting and rich playground to study the complex interplay among spin, charge, orbital, and lattice degrees of freedom [1–6]. Importantly, various physical properties of RVO_3 are strongly coupled with the spin ordered and orbital ordered (OO) states, which depend on the ionic radii of the R ions [7]. In distorted orthovanadates, the V^{3+} ions present in the octahedral coordination sites undergo crystal field splitting, which results in the occupation of two valence electrons in the triply degenerated t_{2g} orbitals. In the low-temperature Jahn-Teller (JT) ordered state, the tetragonal distortion of the V^{3+} octahedra leads to the splitting of the t_{2g} orbitals into a singlet of higher energy and a doublet of lower energy. The doublet contains the d_{xy} orbital, which always remains occupied, and either the d_{zx} or the d_{yz} orbital, which would be occupied alternately on the adjacent V^{3+} sites, giving rise to an OO state [3,8]. In RVO_3, so-called G- and C-type orbital ordering have been observed from various experimental techniques [9–11]. In G-type orbital ordering, the d_{zx} and d_{yz} orbitals are alternately occupied along the three orthogonal directions, whereas in C-type orbital ordering, the d_{zx} and d_{yz} orbitals are alternately occupied in the ab plane and similar orbitals (either d_{zx} or d_{yz}) are occupied along the c direction, as shown schematically in Fig. 1 [5]. The appearance of the G-type orbital ordered (G-OO) state is accompanied by a change in the crystal symmetry from orthorhombic (space group $Pnma$) to monoclinic (space group $P112_1/a$; $\gamma \neq 90^\circ$, c is the unique axis). In the C-type orbital ordered (C-OO) state, the orthorhombic symmetry is preserved except that there exists long and short V-O bond lengths, which alternate along the [110] and [1 $\bar{1}$ 0] directions of the ab plane due to Jahn-Teller distortion. However, in the orbital disordered state with orthorhombic symmetry, all V-O distances in the ab plane are nearly the same [12]. Interestingly, due to the strong coupling between spin ordered and OO states [13] and the Goodenough-Kanamori-Anderson (GKA) rule [14,15], G-OO favors C-type antiferromagnetic (C-AF) ordering, while C-OO leads to G-type antiferromagnetic (G-AF) ordering, as shown in Fig. 1.

The RVO_3 compounds exhibit an orbital disordered orthorhombic structure ($Pnma$) at room temperature but strongly differ at lower temperatures, where various complex spin ordered and OO configurations are observed depending on the R ions. For larger R ions, R = La-Nd, the ground state configuration of RVO_3 is G-OO/C-AF, while the R ions with intermediate ionic radius (Sm–Tb) exhibit a further but partial phase transition from the G-OO (monoclinic) phase to the C-OO (orthorhombic) phase at T_N, below which both phases coexist down to the lowest temperature. However, compounds with a smaller ionic radius (R = Dy-Lu and Y) were reported to undergo a complete phase transition from G-OO/C-AF to C-OO/G-AF far below T_N due to the increase in magnitude of the octahedral tilting of the VO_6 octahedra [7,16].

For example, upon lowering the temperature, Blake *et al.* [17] reported that single crystal YVO_3 shows the orbital disordered orthorhombic phase ($Pnma$) down to 200 K, followed by the G-OO monoclinic phase ($P112_1/a$) in the region of 200–77 K. Below 77 K, the C-OO orthorhombic phase ($Pnma$) is found to be present without evidence of phase coexistence. It has been reported that YVO_3 undergoes long-range antiferromagnetic ordering at 116 K but without accompanying change in the crystal structure, according to Ref. [17]. However, a recent report on $TmVO_3$ unambiguously demonstrated the appearance of the C-OO orthorhombic phase at T_N and its coexistence with the G-OO monoclinic phase between $T_N \sim 105$ K and $T_S \sim 75$ K [18]. The occurrence of the C-OO phase at T_N and its evolution are suggested to be

*Corresponding author: sundaresan@jncasr.ac.in

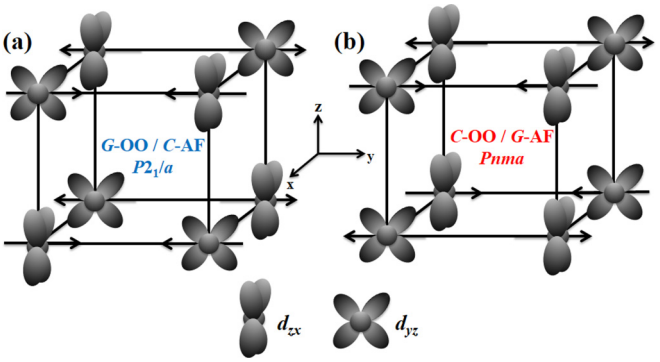

FIG. 1. Schematic representation of (a) G-OO and (b) C-OO states in $R\mathrm{VO}_3$ with the ideal cubic perovskite axes, respectively. The arrows indicate the directions of the magnetic moment on the V^{3+} ion in the magnetically ordered state, where C-AF means that spin ordering is antiferromagnetic only along a and b axes and G-AF means that spin ordering along all three orthogonal directions is antiferromagnetic. For convenience, only occupied d_{zx} and d_{yz} orbitals are shown, while the d_{xy} orbital always remains filled.

triggered by the antiferromagnetic ordering [18]. These results indicate that the phase coexistence is not limited to $R\mathrm{VO}_3$ with intermediate radii of the rare earth cation but instead extends to R ions with lower ionic size. Motivated by these complex structural features, we have investigated various structural phases in YVO_3 using temperature-dependent synchrotron x-ray diffraction (XRD).

Our study reveals the coexistence of the G-OO phase ($P112_1/a$) and the C-OO phase ($Pnma$) in YVO_3 in the temperature range between $T_S \sim 77$ K and $T_N \sim 116$ K, suggesting that the appearance of the C-OO orthorhombic phase at T_N is triggered by the magnetic ordering. It is suggested that the magnetization reversal observed in the temperature range T_S (77 K) $< T < T_N$ (116 K) could be due to different magnetic structures associated with the coexisting G-OO and C-OO phases in the same temperature interval.

II. EXPERIMENTAL DETAILS

Polycrystalline samples of YVO_3 were synthesized in two routes: (1) hydrogen reduction and (2) high-pressure synthesis. In the first method, YVO_3 was synthesized by reducing the YVO_4 under pure H_2(99.9995%) atmosphere at 1400 °C for 24 h with several intermittent grindings to improve the homogeneity of the sample. The polycrystalline powders of YVO_4 were prepared by the conventional solid-state reaction starting from the stoichiometric amounts of binary oxides, $\mathrm{Y}_2\mathrm{O}_3$ (Alfa Aesar, 99.99%) and $\mathrm{V}_2\mathrm{O}_5$ (Sigma Aldrich, 99.99%), which were mixed together, ground, and heated in air at 1000 °C and 1200 °C for the duration of 12 h with intermediate grinding. In addition, we prepared YVO_3 samples under reducing atmosphere at a lower annealing temperature (800 °C). In the second method, a cubic-anvil high-pressure apparatus was used to make YVO_3 from the starting materials, high-purity $\mathrm{Y}_2\mathrm{O}_3$ (Alfa Aesar, 99.99%) and $\mathrm{V}_2\mathrm{O}_3$ (Sigma Aldrich, 99.99%). The stoichiometric powder was encapsulated in boron nitride (BN) capsule, kept in a closed container made of a BN sleeve, and then placed into a solid pyrophyllite cube, which transmit pressure from the surrounding anvils. The sample was prepared by applying a pressure of ~4.5 GPa and temperature of 1000 °C.

The phase purity of the polycrystalline YVO_3 sample was confirmed by acquiring XRD data at room temperature with the PANalytical Empyrean diffractometer using monochromatic Cu Kα_1. The variable temperature synchrotron XRD data of YVO_3 were collected with the wavelengths 0.3171, 0.4762, or 0.4127 Å on the material science powder diffraction beamline (BL04-MSPD) of the ALBA synchrotron facility [19,20]. Samples were cooled using the recently developed liquid helium Dynaflow cryostat [21]. The FullProf suite [22] was used to perform Rietveld refinement on the XRD pattern collected as a function of temperature.

Temperature-dependent direct current (dc) magnetization and alternating current (ac) magnetic susceptibility measurements of polycrystalline YVO_3 were carried out using a superconducting quantum interference device (SQUID) magnetometer (MPMS3) and Physical Property Measurement System (PPMS; Quantum Design), respectively. Thermogravimetric analysis (TGA) was carried out with a Perkin-Elmer Pyris1 instrument. About 20–30 mg of sample were loaded into a furnace using a platinum crucible and heated to the target temperature at a rate of 10 °C/min.

III. RESULTS AND DISCUSSION

Since most of the polycrystalline $R\mathrm{VO}_3$ compounds reported in the literature are prepared by hydrogen reduction of $R\mathrm{VO}_4$, we will present our results and discuss the hydrogen-reduced YVO_3 sample. Analysis of synchrotron data collected at the ambient condition confirmed that the compound YVO_3 crystallizes in the orthorhombic structure with the space group $Pnma$, as reported earlier [4]. However, we found that the profiles of the reflections (200, 220, 202, 321, ...) and (022, 040, 042, 004, 161, ...) are highly asymmetric, with a Lorentzian tail on the side of higher and lower angles, respectively. In the absence of lowering of symmetry, such hkl-dependent asymmetric broadening could indicate a possible anisotropic strain distribution, which is rarely treated quantitatively. Therefore, we have modeled the diffraction data with a distribution of lattice parameters within the orthorhombic structure ($Pnma$) [23,24]. We have performed Rietveld refinement using two similar sets of lattice parameters in the $Pnma$ space group (Fig. 2). As seen in the inset of Fig. 2, our phenomenological two-phase model correctly simulates the asymmetric character of high intensity peaks (200) and (210). Better refinement reliability factors are obtained by increasing the number of refined phases. However, to obtain reasonable structural parameters, only two sets of lattice parameters were used. The structural parameters obtained from the Rietveld refinement of ambient condition XRD data are shown in Table I. Since the thermogravimetric analysis suggests that the oxygen content of the sample is close to stoichiometric (~2.97 ± 0.02), the asymmetric nature of the peaks could be related to the fact that the samples are prepared from $R\mathrm{VO}_4$ by reducing under a hydrogen atmosphere. This observation prompted us to check the role of the synthetic condition on the asymmetry and thus the distribution of the lattice parameters throughout the sample.

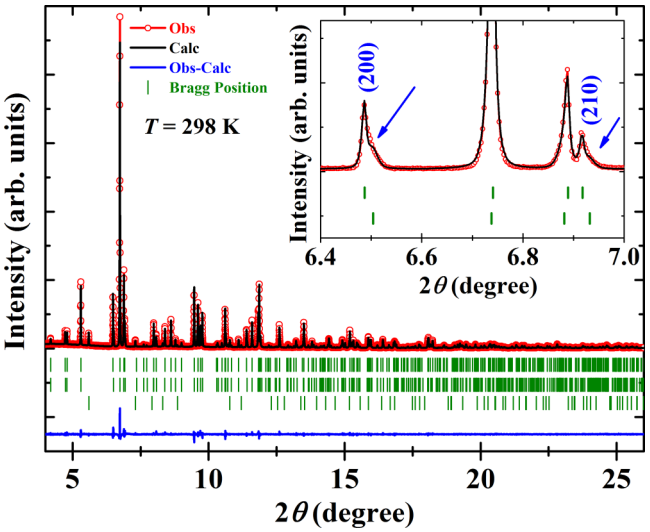

FIG. 2. Rietveld refinement of synchrotron XRD pattern of polycrystalline YVO_3 at 298 K using a wavelength of $\lambda = 0.3171$ Å. Inset shows the enlarged view of Bragg peaks across the highest intensity to reveal the asymmetry in the (200) and (210) peaks (indicated by an arrow). The first two Bragg positions are associated with the two different sets of lattice parameters under the space group *Pnma*, and the last Bragg positions are associated with TiO_2 (Rutile phase) originated from the cryostat.

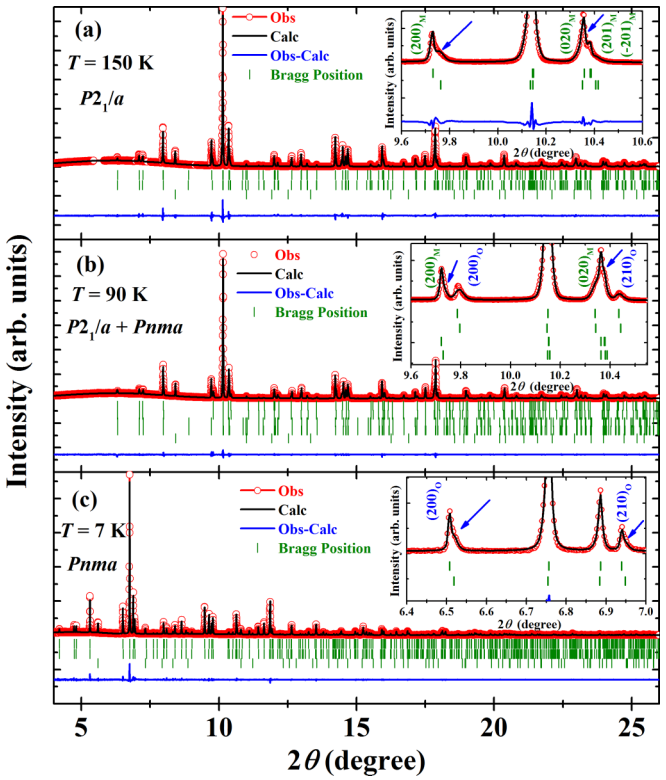

FIG. 3. Rietveld refinement of the temperature-dependent synchrotron XRD pattern of polycrystalline YVO_3 at (a) 150 K, (b) 90 K, and (c) 7 K using wavelengths of $\lambda = 0.4762$ Å (a and b) and 0.3171 Å (c). Inset of (a)–(c) shows the enlarged view of Bragg peaks across the highest intensity to reveal the asymmetry in the (200), (210), and (201) peaks (indicated by an arrow). For each space group, two sets of lattice parameters have been used and hence two Bragg positions. The last Bragg positions in each panel are due to the TiO_2 (Rutile phase) originated from the cryostat. In the insets, the suffixes O and M outside the parentheses stand for orthorhombic and monoclinic symmetry, respectively. Small excluded peaks in (a) that are visible in the 2θ range of 5°–6° originate from the cryostat.

The peak asymmetry in the sample prepared at a lower annealing temperature (800 °C) is almost negligible, as shown in Supplemental Material Fig. S1 [25]. This suggests that the asymmetry depends on the synthetic condition.

We see similar asymmetry in the room temperature XRD pattern of other RVO_3 compounds with intermediate-size rare earth ions (R = Sm, Eu, Gd, and Tb) prepared at 1400 °C, as shown in Supplemental Material Fig. S2 [25]. Such an asymmetric broadening is also reported in the synchrotron data of $GdVO_3$ collected at 295 K [7]. From Ref. [6], we

TABLE I. Structural parameters of YVO_3 at 298 K.

Space group: *Pnma* (orthorhombic)					
Phase I [59.32 (0.63)%]					
$a = 5.60413(1)$ Å, $b = 7.57320(2)$ Å, $c = 5.27781(1)$ Å					
Atom (position)	x	y	z	B_{iso}(Å^2)	Occupancy
Y (4*c*)	0.0689 (1)	0.25	0.9798 (2)	0.39 (2)	1.0
V (4*b*)	0	0	0.5	0.31 (3)	1.0
O1 (4*c*)	0.4538 (12)	0.25	0.1135 (14)	0.42 (5)	1.0
O2 (8*d*)	0.3028 (9)	0.0595 (8)	0.6907 (11)	0.42 (5)	1.0
$R_B = 3.24\%, R_F = 3.59\%, \chi^2 = 1.94\%$					
Phase II [40.68 (0.58)%]					
$a = 5.59020(6)$ Å, $b = 7.58275(7)$ Å, $c = 5.28285(5)$ Å					
Atom (position)	x	y	z	B_{iso}(Å^2)	Occupancy
Y (4*c*)	0.0684 (3)	0.25	0.9835 (5)	0.55 (4)	1.0
V (4*b*)	0	0	0.5	0.84 (6)	1.0
O1 (4*c*)	0.4726 (19)	0.25	0.0979 (24)	0.42 (5)	1.0
O2 (8*d*)	0.3079 (16)	0.0529 (13)	0.6857 (19)	0.42 (5)	1.0
$R_B = 3.86\%, R_F = 3.45\%, \chi^2 = 1.94\%$					

TABLE II. Structural parameters of YVO_3 at 150 K.

Space group: $P112_1/a$ (monoclinic)					
Phase I [58.87 (0.51)%]					
$a = 5.61514(2)$ Å, $b = 7.54711(3)$ Å, $c = 5.27571(2)$ Å; $\gamma = 89.9699(7)^\circ$					
Atom (position)	x	y	z	B_{iso}(Å^2)	Occupancy
Y ($4e$)	0.0708 (1)	0.2489 (5)	0.9801 (3)	0.15 (1)	1.0
V1 ($2c$)	0.5	0	0	0.21 (2)	1.0
V2 ($2b$)	0	0.5	0.5	0.21 (2)	1.0
O1 ($4e$)	0.4560 (14)	0.2509 (37)	0.1155 (17)	1.00	1.0
O2 ($4e$)	0.3045 (28)	0.0629 (26)	0.6971 (46)	1.00	1.0
O3 ($4e$)	0.7050 (27)	0.5548 (26)	0.3141 (48)	1.00	1.0
$R_B = 4.57\%, R_F = 3.79\%, \chi^2 = 4.86\%$					
Phase II [41.13 (0.45)%]					
$a = 5.59714(7)$ Å, $b = 7.56388(8)$ Å, $c = 5.27971(6)$ Å; $\gamma = 89.9139(18)^\circ$					
Atom (position)	x	y	z	B_{iso}(Å^2)	Occupancy
Y ($4e$)	0.0681 (2)	0.2482 (6)	0.9781 (4)	0.15 (1)	1.0
V1 ($2c$)	0.5	0	0	0.21 (2)	1.0
V2 ($2b$)	0	0.5	0.5	0.21 (2)	1.0
O1 ($4e$)	0.4599 (20)	0.2247 (46)	0.1001 (27)	1.00	1.0
O2 ($4e$)	0.3212 (46)	0.0450 (33)	0.6901 (45)	1.00	1.0
O3 ($4e$)	0.7124 (47)	0.5709 (34)	0.3330 (50)	1.00	1.0
$R_B = 7.86\%, R_F = 4.67\%, \chi^2 = 4.86\%$					

can clearly see the asymmetric broadening of the (321) reflection [considering $Pnma$ symmetry], which has not been accounted by the authors. We see similar asymmetry of the (321) reflection in YVO_3 (as well as in $GdVO_3$), which we have modeled with the lattice parameter distribution that improved the goodness of fit, as shown in Supplemental Material Fig. S3 [25].

Since we observe distribution of lattice parameters in YVO_3 at ambient conditions, we expect such lattice parameter distribution would also be present at low temperatures. Keeping this in mind, we collected synchrotron XRD data at several low temperatures, and the results of Rietveld refinement at 150, 90, and 7 K are shown in Figs. 3(a), 3(b), and 3(c), respectively. As expected, all these data show asymmetry on the above-mentioned Bragg peaks, indicating the presence of lattice parameter distribution. Consequently, the 150 K data could be modeled with the G-OO monoclinic structure ($P112_1/a$) as reported earlier but with a lattice parameter distribution [Fig. 3(a)]. At 7 K, the data are consistent with the C-OO orthorhombic phase ($Pnma$), which is in agreement with the earlier report that C-OO occurs at $T_S \sim 77$ K but with two different sets of lattice parameters. Interestingly, at 90 K (below $T_N = 116$ K), we observe that the G-OO monoclinic phase ($P112_1/a$) coexists with the C-OO orthorhombic phase ($Pnma$). Both phases require the model of lattice parameter distribution to obtain a best fit to the observed data. Such a phase coexistence in YVO_3 is not known in the literature except for Raman spectroscopic study, which suggest only a short-range correlation or fluctuation of the C-OO state coexisting with the G-OO state [26]. From the Rietveld analysis of temperature-dependent diffraction data, we observe that such a phase coexistence, which arises near T_N, remains down to the second structural transition at $T_S \sim 77$ K, below which the G-OO phase converts to a single orthorhombic phase ($Pnma$) with the C-OO state. This observation is in agreement with the recent report on $TmVO_3$ [18]. The obtained structural parameters from the Rietveld refinement of 150 and 90 K data are displayed in Tables II and III, respectively. The (200) reflection, which consists of the characteristics of distribution of the cell parameters, is found to be asymmetric at all temperatures [inset of Fig. 3]. The structural parameters extracted from the refinement of 7 K data are shown in Table IV. In Fig. 4, we show the evolution of temperature-dependent phase fractions, which clearly reveals that phase coexistence between the G-OO monoclinic phase ($P112_1/a$) and the C-OO orthorhombic phase ($Pnma$) persists in the temperature range $T_S\,(77\,\text{K}) < T < T_N\,(116\,\text{K})$. Below T_S, only the C-OO orthorhombic phase ($Pnma$) exists.

We discuss below that the phase coexistence correlates with the temperature-induced magnetization reversal observed in the same temperature interval, $T_S\,(77\,\text{K}) < T < T_N\,(116\,\text{K})$. The temperature dependence of dc and ac magnetization measured in polycrystalline YVO_3 samples is shown in Fig. 5(a). From this figure, it is evident that the onset of phase coexistence is concomitant with the Néel temperature ($T_N \sim 116$ K) and the disappearance of phase coexistence coincides with the magnetization anomaly at $T_S \sim 77$ K, below which only the C-OO phase exists. Interestingly, in the phase-coexisting temperature range $T_S\,(77\,\text{K}) < T < T_N\,(116\,\text{K})$, multiple temperature-induced magnetization reversal phenomena have been reported in a single crystal YVO_3 in the presence of modest magnetic fields ($H = 1$ kOe) applied along the crystallographic a axis [2]. We also observe such magnetization reversal in the polycrystalline sample only in oriented grains under the magnetic field, as shown in Fig. 5(b). In Ref. [2], the phenomenon of magnetization reversal has been explained based on a microscopic model considering the competing single-ion anisotropy and Dzyaloshinskii-Moriya (DM) coupling. However, according to Néel's prediction [27], in

TABLE III. Structural parameters of YVO_3 at 90 K.

Space group: $P112_1/a$ (monoclinic) [85.31 (0.88)%]					
$a = 5.62036(2)$ Å, $b = 7.53460(3)$ Å, $c = 5.27336(2)$ Å; $\gamma = 90.0139(9)^\circ$					
Atom (position)	x	y	z	B_{iso}(Å^2)	Occupancy
Y (4e)	0.0709 (2)	0.2501 (8)	0.9834 (3)	1.63 (3)	1.0
V1 (2c)	0.5	0	0	1.51 (5)	1.0
V2 (2b)	0	0.5	0.5	1.51 (5)	1.0
O1 (4e)	0.4327 (17)	0.2668 (26)	0.1280 (17)	1.00	1.0
O2 (4e)	0.2884 (35)	0.0548 (27)	0.6826 (29)	1.00	1.0
O3 (4e)	0.6920 (38)	0.5619 (26)	0.2627 (32)	1.00	1.0
$R_B = 2.04\%, R_F = 1.47\%, \chi^2 = 1.90\%$					
Space group: $Pnma$ (orthorhombic) [14.69 (0.43)%]					
$a = 5.58359(11)$ Å, $b = 7.55268(16)$ Å, $c = 5.28533(15)$ Å					
Atom (position)	x	y	z	B_{iso}(Å^2)	Occupancy
Y (4c)	0.0680 (11)	0.25	0.9769 (32)	1.63 (3)	1.0
V (4b)	0	0	0.5	1.51 (5)	1.0
O1 (4c)	0.5923 (88)	0.25	0.3979 (98)	1.00	1.0
O2 (8d)	0.2397 (92)	0.0257 (71)	0.7125 (71)	1.00	1.0
$R_B = 2.32\%, R_F = 2.08\%, \chi^2 = 1.90\%$					

some ferrimagnetic systems, the temperature dependence of each sublattice can vary independently, which results in magnetization reversal, as observed experimentally in CoV_2O_4, and this mechanism is successful in explaining the magnetization reversal in several ferrimagnetic systems [28–30]. Since vanadium ions in YVO_3 exist in only one oxidation state (V^{3+}), we cannot explain the observed magnetization reversal in YVO_3 based on Néel's two-sublattice model. From the present study, we suggest that the temperature evolution of magnetization associated with the two coexisting phases in the region can vary independently, which could explain the magnetization reversal. We find that the correlation between phase coexistence and magnetization reversal exists not only in YVO_3 but also in other RVO_3 systems.

In $LaVO_3$, the magnetization reversal is reported to remain down to the lowest temperature at which the phase coexistence was evidenced from Raman spectroscopy [31,32]. In the case of $SmVO_3$, though the phase coexistence remains down to the lowest temperature [16], the magnetization changes continuously from negative to positive because the paramagnetic moment of Sm^{3+} ions dominates at low temperatures [31]. However, in the RVO_3 system with smaller R ions, where the phase coexistence is present only in a certain temperature interval and irrespective of whether the R ion is paramagnetic, there is a sharp change in magnetization from negative to positive at T_S because the phase coexistence disappears abruptly at this temperature, as observed in YVO_3 and $TmVO_3$ [18]. The magnetization reversal and the phase coexistence are not known in $LuVO_3$ [33]. In order to confirm the temperature variation of the magnetic moment across the phase-coexisting region, it requires a high-resolution neutron diffraction measurement. Though we have suggested that mag-

TABLE IV. Structural parameters of YVO_3 at 7 K.

Space group: $Pnma$ (orthorhombic)					
Phase I [49.24 (0.80)%]					
$a = 5.58702(2)$ Å, $b = 7.54766(2)$ Å, $c = 5.28008(2)$ Å					
Atom (position)	x	y	z	B_{iso}(Å^2)	Occupancy
Y (4c)	0.0706 (2)	0.25	0.9781 (2)	0.47 (2)	1.0
V (4b)	0	0	0.5	0.46 (3)	1.0
O1 (4c)	0.4567 (15)	0.25	0.1177 (16)	0.74 (4)	1.0
O2 (8d)	0.2990 (12)	0.0579 (9)	0.6905 (14)	0.74 (4)	1.0
$R_B = 4.27\%, R_F = 2.43\%, \chi^2 = 1.4\%$					
Phase II [50.76 (0.85)%]					
$a = 5.57755(6)$ Å, $b = 7.55703(8)$ Å, $c = 5.28179(5)$ Å					
Atom (position)	x	y	z	B_{iso}(Å^2)	Occupancy
Y (4c)	0.0698 (2)	0.25	0.9799 (4)	0.54 (3)	1.0
V (4b)	0	0	0.5	0.88 (5)	1.0
O1 (4c)	0.4671 (19)	0.25	0.0987 (23)	0.74 (4)	1.0
O2 (8d)	0.2996 (15)	0.0563 (12)	0.6812 (19)	0.74 (4)	1.0
$R_B = 4.58\%, R_F = 2.32\%, \chi^2 = 1.4\%$					

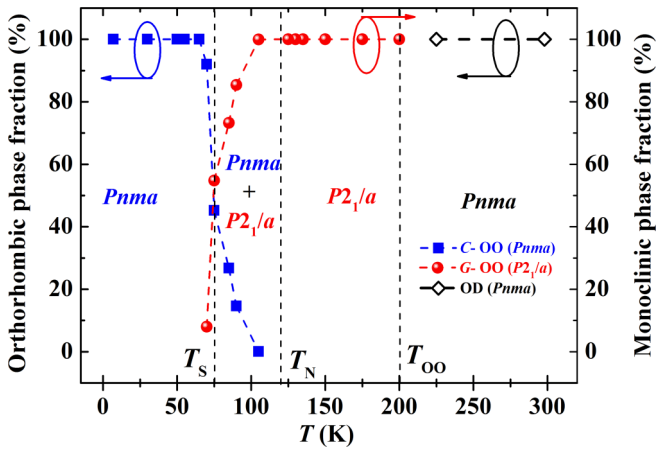

FIG. 4. Variation of phase fractions of orthorhombic and monoclinic structures of polycrystalline YVO_3 as a function of temperature.

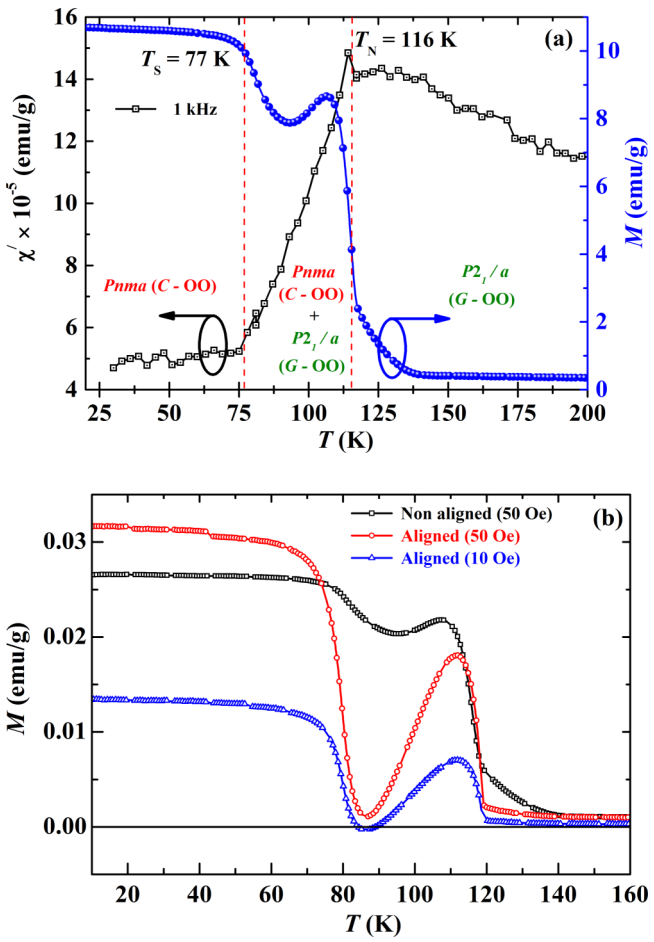

FIG. 5. (a) Temperature-dependent dc magnetization data measured under a magnetic field of 100 Oe (right) and the real part of ac magnetic susceptibility with an ac amplitude of 10 Oe (left) for polycrystalline YVO_3. (b) Temperature dependence of field-cooled (FC) dc magnetization data of polycrystalline YVO_3 at different magnetic fields after aligning the grain under a magnetic field of 10 kOe.

netic phase coexistence could be related to the magnetization reversal, it requires a microscopic understanding.

In Fig. 6, we show the variation of lattice parameters and unit cell volume as a function of temperature. From this figure, we can see that there is a change in slope in all three lattice parameters at T_{OO}, T_N, and T_S. Temperature-dependent volume data [Fig. 6(d)] show a monotonous decrease with lowering temperature followed by a jump at $T_N \sim 116$ K, indicating a first-order phase transition associated with the coexistence of crystallographic phases of monoclinic ($P112_1/a$) and orthorhombic ($Pnma$) symmetry. Interestingly, both b and c lattice parameters decrease while the a parameter increases with lowering of the temperature in the region 200–100 K. This anisotropic expansion and contraction could be understood from the variation of the V-O bonding pattern of the VO_6 octahedra, as shown in Fig. 7(a). The anisotropic lattice parameter suggests that there would be two pairs of short and one pair of long V-O bonds, which are indications of the Jahn-Teller ordered state. In $Pnma$ settings, the equatorial ac plane of the VO_6 octahedra would contain two long and two short V-O_2 bonds. The second pair of short bonds (V-O_1) would be along the apical b axis. In spite of the fact that determination of V-O bond length would involve a larger standard deviation compared to the results obtained from the neutron diffraction experiment, qualitatively the obtained bond lengths agree with the reported literature [17]. From Fig. 7(a), it is evident that at the onset of the G-OO state ($T_{OO} \sim 200$ K), the six bonds of the VO_6 octahedra are split into two short and two long bonds in the ac plane, suggesting that orbital degeneracy of the t_{2g} orbital of the V^{3+} (d^2) ion is lifted. In contrast, there would be three inequivalent V-O bonds at all temperatures above the Jahn-Teller transition temperature ($T_{OO} \sim 200$ K). We also observe a jump in apical V-O_1 bond distance around 90 K, which could be due to the sudden change in the tilt of the octahedra. Interestingly, the abrupt change in V-O_1 bond length around 90 K is reflected in the sudden change in V-O_1-V bond angle, as shown in Fig. 7(b). In YVO_3, octahedral distortion increases with lowering temperature, and it becomes the maximum around 90 K. We have seen from Fig. 7(a) that the apical V-O_1 bond distance (along the b axis) of the VO_6 octahedra peaks around 90 K and then decreases, which indicates a sudden increase in octahedral tilting followed by relief from the octahedral distortion. Accordingly, phase coexistence, which nucleates at T_N, suggests that the upper stability limit to support octahedral tilting by the $P112_1/a$ phase has probably reached a maximum limit near 90 K; therefore to provide relief from that, some portion of the $P112_1/a$ phase converts to the C-OO $Pnma$ phase.

Now we discuss the orbital phase coexistence observed in the temperature range of $T_S < T < T_N$. Sage *et al.* have constructed a phase diagram on the stability of G-OO and C-OO states in RVO_3 based on the opposing influence of octahedral distortion and the magnetic exchange interaction [7]. From the phase diagram, it is evident that with increasing octahedral distortion C-OO is preferred, while with increasing magnetic exchange striction the G-OO state is stabilized. In our study of YVO_3, we find that the monoclinic phase with the G-OO state appears at ~200 K and then with lowering temperature the octahedral tilting increases, leading to the appearance of the C-OO state with $Pnma$ symmetry around $T_N \sim 116$ K in the background of the monoclinic phase

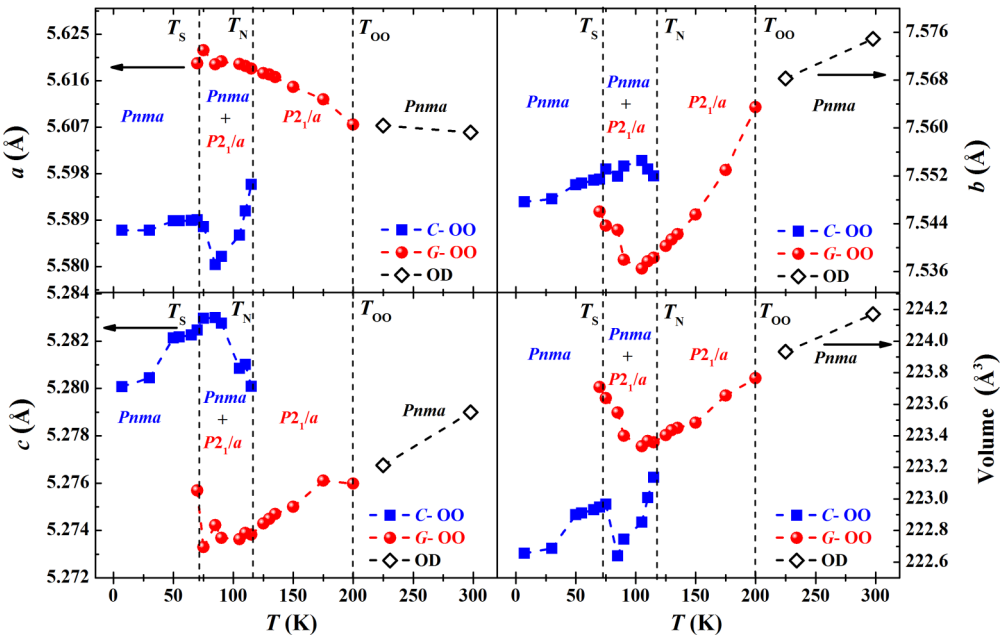

FIG. 6. Variation of lattice parameters and unit cell volume of polycrystalline YVO_3 as a function of temperature.

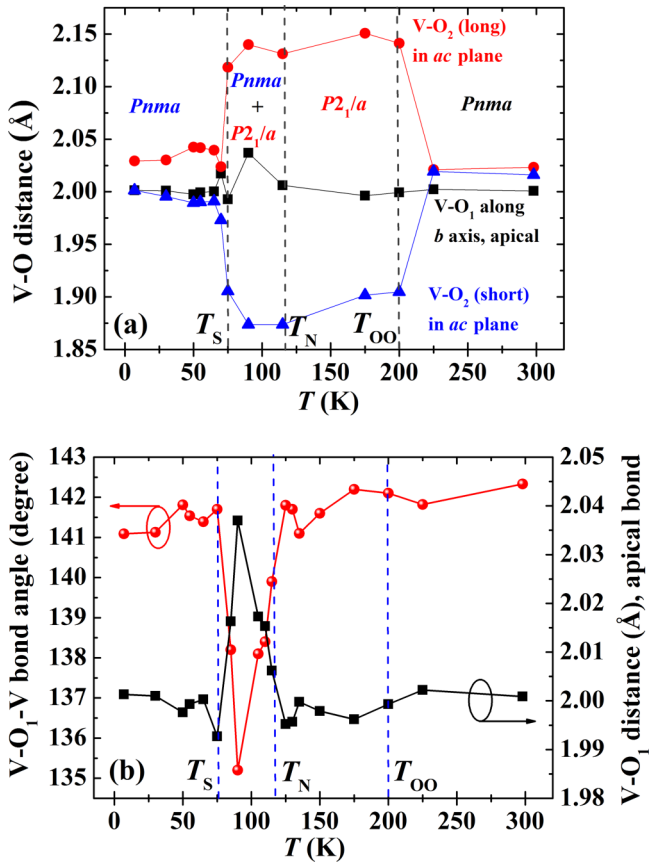

FIG. 7. Temperature-dependent (a) V-O bond distances and (b) V-O_1-V bond angles of polycrystalline YVO_3 obtained from the Rietveld refinement of the synchrotron XRD pattern (standard error of the data would be high due to the inability of XRD to determine the position of the oxygen atom accurately in the presence of dominating scattering from the Y^{3+} ion).

($P112_1/a$), thereby creating phase coexistence. The phase coexistence starts at T_N because the octahedral distortion, which increases with lowering temperature, facilitates the gain in exchange energy at the magnetic ordering as a result of magnetostructural coupling. The concurrent appearance of the *C*-OO state (*Pnma*) with the magnetic ordering is considered the magnetostructural effect. In addition, the gain in exchange energy at T_N will facilitate the ability to overcome the elastic energy cost of the octahedral distortion,

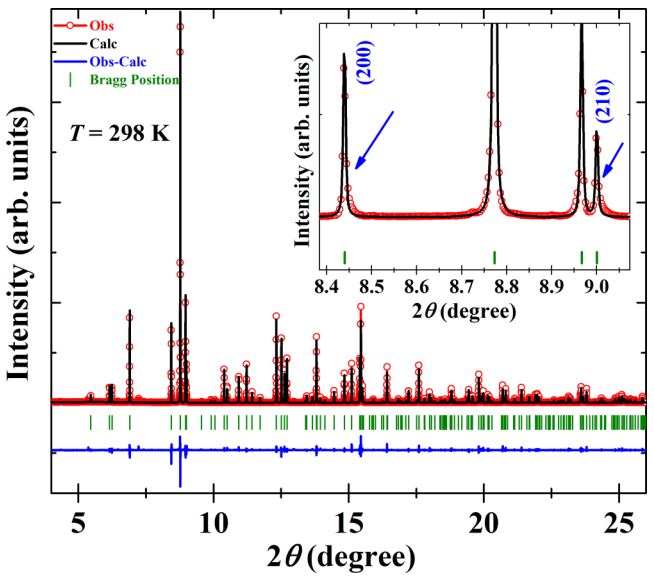

FIG. 8. Rietveld refinement of room temperature synchrotron XRD pattern of polycrystalline YVO_3 prepared at 1000 °C under high pressure using a wavelength of $\lambda = 0.4127$ Å. Inset shows the enlarged view of Bragg peaks across the highest intensity to reveal the negligible asymmetry in the (200) and (210) peaks (indicated by an arrow). The small unfitted peak visible in the 2θ range of 7.1°–7.5° is associated with small impurity.

TABLE V. Structural parameters of YVO_3 synthesized under high pressure at 298 K.

Space group: $Pnma$ (orthorhombic) $a = 5.60846(1)$ Å, $b = 7.57459(1)$ Å, $c = 5.27951(1)$ Å					
Atom (position)	x	y	z	B_{iso}(Å^2)	Occupancy
Y (4c)	0.0694 (1)	0.25	0.9800 (1)	0.23 (1)	1.0
V (4b)	0	0	0.5	0.34 (2)	1.0
O1 (4c)	0.4612 (8)	0.25	0.1127 (8)	1.00 (0)	1.0
O2 (8d)	0.3030 (6)	0.0558 (4)	0.6914 (6)	1.00 (0)	1.0
$R_B = 6.44\%, R_F = 5.84\%, \chi^2 = 6.54\%$					

thereby making the whole process energetically favorable. In contrast to the RVO_3 compounds with intermediate-size rare earth ions (R = Sm, Eu, Gd, and Tb), where the phase coexistence appearing just below T_N remains down to the lowest temperature (5 K), the phase coexistence in YVO_3 survives only in the temperature window between T_N and T_S. The occurrence of phase coexistence in the orthovanadates with intermediate rare earth has been attributed to the magnetic exchange striction, which leads to the change in volume in the vicinity of T_N [7]. In YVO_3, we could correlate the origin of phase coexistence of G-OO and C-OO states in terms of recent observation on $TmVO_3$, where the occurrence of two different coexisting magnetic structures is associated with the nuclear phase $P112_1/a$ and another magnetic structure is associated with the nuclear phase $Pnma$ in the temperature region of $T_S < T < T_N$, suggested to be responsible for phase coexistence [18]. In order to verify whether the observed asymmetry on selected Bragg peaks or some oxygen vacancy could be responsible for the phase coexistence, we have prepared a polycrystalline YVO_3 sample by high-pressure (∼4.5 GPa) synthesis starting from stoichiometric mixtures of Y_2O_3 and V_2O_3 as described in Sec. II. High-pressure synthesis is an effective tool to control the oxygen content in the sample. In Fig. 8, we show the Rietveld refinement of the room temperature synchrotron XRD pattern of YVO_3 prepared under high pressure, and the corresponding structural parameters are displayed in Table V. This sample did not show significant asymmetry but showed phase coexistence. This result suggests that the origin of phase coexistence is not related to asymmetry in the XRD peak or oxygen vacancy. Even if we consider some oxygen vacancy, it cannot result in the coexistence of G-OO and C-OO phases, because both phases require orbital degeneracy, i.e., the Jahn-Teller active electronic configuration of the vanadium ion. The stoichiometric sample should have the V^{3+} ion with the d^2 Jahn-Teller active electronic configuration, whereas the V^{2+} ion (due to oxygen deficiency) with the d^3 electronic configuration is non-Jahn-Teller active and has no orbital degeneracy. Therefore, the observed phase coexistence should arise from the stoichiometric sample.

Such phase separation into OO states (G- and C-type) of different structural symmetry in $T_S < T < T_N$ is analogous to the occurrence of electronic phase coexistence between metallic and insulating phases in doped rare earth manganites, where the origin of this phenomena has been attributed to the strong electron-lattice coupling and the presence of long-range strain [34]. In RVO_3 compounds, with intermediate-size rare earth ions (R = Sm, Eu, Gd, and Tb), orbital phase coexistence has been attributed to the lattice strain associated with the difference in unit cell volume of orthorhombic (C-OO) and monoclinic (G-OO) phases, and the strain present in the system prevents complete phase transformations, thereby allowing the phase coexistence to prevail until 5 K [7,16]. Analogous to the magnetically phase-separated mixed valent rare earth manganites, where ferromagnetic metallic puddles grow on the matrix of an insulating antiferromagnetic background, it can be inferred that in YVO_3, the competition between ordering of different orbital states favors the formation of one particular type of orbital ordering over the background of another OO state, leading to orbital phase separation into G- and C-type. The coupling between different orbital states is mediated by the lattice; therefore, the change in orbital state would be reflected on lattice symmetry. With decreasing temperature, due to reduction in unit cell volume, the C-OO state ($Pnma$) evolves in the regime of the G-OO state as a result of increased octahedral distortion, facilitating release of the strain. The relaxation of strain is reflected in the reduction of unit cell volume with decreasing temperature [Fig. 6(d)], indicating the occurrence of the first-order orbital phase transition.

IV. CONCLUSIONS

Using high-angular-resolution synchrotron x-ray powder diffraction, we have shown that the high-temperature G-OO monoclinic phase ($P112_1/a$) and the low-temperature C-OO orthorhombic phase ($Pnma$) coexist in the temperature interval $T_S < T < T_N$. The onset of the C-OO state at T_N is attributed to the magnetostructural coupling due to large distortion of the VO_6 octahedra facilitating the gain in exchange energy. It is suggested that the coexistence of the two magnetic phases associated with the coexisting G-OO and C-OO phases is responsible for the temperature-induced magnetization reversal observed in the phase-coexisting region in YVO_3 and, in general, the magnetization reversal observed in other RVO_3 systems.

ACKNOWLEDGMENTS

The authors thank P. Mandal for his help during the magnetic measurement. A.S. acknowledges Sheikh Saqr Laboratory (SSL) at Jawaharlal Nehru Centre for Advanced Scientific Research (JNCASR). R.S. thanks JNCASR for providing a Ph.D. scholarship (JNC/S0154) and SSL for the research associate fellowship (JNC/SSL/CNR/6001).

[1] S. Miyasaka, Y. Okimoto, M. Iwama, and Y. Tokura, Phys. Rev. B **68**, 100406 (2003).

[2] Y. Ren, T. Palstra, D. Khomskii, E. Pellegrin, A. Nugroho, A. Menovsky, and G. Sawatzky, Nature **396**, 441 (1998).

[3] J. B. Goodenough and J.-S. Zhou, J. Mater. Chem. **17**, 2394 (2007).

[4] M. Reehuis, C. Ulrich, P. Pattison, B. Ouladdiaf, M. C. Rheinstädter, M. Ohl, L. P. Regnault, M. Miyasaka, Y. Tokura, and B. Keimer, Phys. Rev. B **73**, 094440 (2006).

[5] T. Mizokawa, D. I. Khomskii, and G. A. Sawatzky, Phys. Rev. B **60**, 7309 (1999).

[6] E. Benckiser, L. Fels, G. Ghiringhelli, M. Moretti Sala, T. Schmitt, J. Schlappa, V. N. Strocov, N. Mufti, G. R. Blake, A. A. Nugroho, T. T. M. Palstra, M. W. Haverkort, K. Wohlfeld, and M. Grüninger, Phys. Rev. B **88**, 205115 (2013).

[7] M. H. Sage, G. R. Blake, C. Marquina, and T. T. M. Palstra, Phys. Rev. B **76**, 195102 (2007).

[8] J. Goodenough, Annu. Rev. Mater. Sci. **28**, 1 (1998).

[9] D. Bizen, N. Shirane, T. Murata, H. Nakao, Y. Murakami, J. Fujioka, T. Yasue, S. Miyasaka, and Y. Tokura, J. Phys.: Conf. Ser. **150**, 042010 (2009).

[10] S. B. Wilkins, P. D. Spencer, P. D. Hatton, S. P. Collins, M. D. Roper, D. Prabhakaran, and A. T. Boothroyd, Phys. Rev. Lett. **91**, 167205 (2003).

[11] Y. Murakami, J. P. Hill, D. Gibbs, M. Blume, I. Koyama, M. Tanaka, H. Kawata, T. Arima, Y. Tokura, K. Hirota, and Y. Endoh, Phys. Rev. Lett. **81**, 582 (1998).

[12] G. R. Blake, T. T. M. Palstra, Y. Ren, A. A. Nugroho, and A. A. Menovsky, Phys. Rev. Lett. **87**, 245501 (2001).

[13] D. Bizen, H. Nakao, K. Iwasa, Y. Murakami, T. Osakabe, J. Fujioka, T. Yasue, S. Miyasaka, and Y. Tokura, J. Phys. Soc. Jpn. **81**, 024715 (2012).

[14] J. Kanamori, J. Phys. Chem. Solid. **10**, 87 (1959).

[15] P. W. Anderson, Solid State Phys. **14**, 99 (1963).

[16] M. H. Sage, G. R. Blake, G. J. Nieuwenhuys, and T. T. M. Palstra, Phys. Rev. Lett. **96**, 036401 (2006).

[17] G. R. Blake, T. T. M. Palstra, Y. Ren, A. A. Nugroho, and A. A. Menovsky, Phys. Rev. B **65**, 174112 (2002).

[18] C. Ritter, S. A. Ivanov, G. V. Bazuev, and F. Fauth, Phys. Rev. B **93**, 054423 (2016).

[19] F. Fauth, I. Peral, C. Popescu, and M. Knapp, Powder Diffr. **28**, S360 (2013).

[20] F. Fauth, R. Boer, F. Gil-Ortiz, C. Popescu, O. Vallcorba, I. Peral, D. Fullà, J. Benach, and J. Juanhuix, Eur. Phys. J. Plus **130**, 160 (2015).

[21] P. J. E. M. van der Linden, M. M. Sala, C. Henriquet, M. Rossi, K. Ohgushi, F. Fauth, L. Simonelli, C. Marini, E. Fraga, C. Murray, J. Potter, and M. Krisch, Rev. Sci. Instrum. **87**, 115103 (2016).

[22] J. Rodríguez-Carvajal, Phys. B Condens. Matter **192**, 55 (1993).

[23] P. Karen, J. Solid State Chem. **170**, 9 (2003).

[24] P. W. Stephens, J. Appl. Crystallogr. **32**, 281 (1999).

[25] See Supplemental Material at http://link.aps.org/supplemental/10.1103/PhysRevB.95.184107 for additional XRD measurements on YVO_3 and other RVO_3(R = Sm, Eu, Gd, and Tb) compounds.

[26] S. Miyasaka, J. Fujioka, M. Iwama, Y. Okimoto, and Y. Tokura, Phys. Rev. B **73**, 224436 (2006).

[27] L. Néel, Ann. Phys. (Paris) **3**, 137 (1948).

[28] N. Menyuk, K. Dwight, and D. Wickham, Phys. Rev. Lett. **4**, 119 (1960).

[29] A. Kumar and S. Yusuf, Phys. Rep. **556**, 1 (2015).

[30] P. Mandal, A. Sundaresan, C. N. R. Rao, A. Iyo, P. M. Shirage, Y. Tanaka, Ch. Simon, V. Pralong, O. I. Lebedev, V. Caignaert, and B. Raveau, Phys. Rev. B **82**, 100416(R) (2010).

[31] L. D. Tung, M. R. Lees, G. Balakrishnan, and D. McK. Paul, Phys. Rev. B **75**, 104404 (2007).

[32] B. Roberge, S. Jandl, A. A. Nugroho, T. Palstra, L. D. Tung, and G. Balakrishnan, J. Raman Spectrosc. **46**, 1157 (2015).

[33] J.-Q. Yan, J.-S. Zhou, and J. B. Goodenough, Phys. Rev. B **72**, 094412 (2005).

[34] K. Ahn, T. Lookman, and A. Bishop, Nature **428**, 401 (2004).